Modeling and numerical study of primary breakup under diesel conditions

Modeling and numerical study of primary breakup under diesel conditions

A. Movaghar[1], M. Linne[2], M. Herrmann[3], A. R. Kerstein[4], M. Oevermann[1]

[1]*Department of Mechanics, Chalmers University of Technology, Gothenburg, Sweden*
[2]*School of Engineering, University of Edinburgh, Edinburgh, UK*
[3]*Department of Mechanical and Aerospace Engineering, Arizona State University, Tempe, Arizona, USA*
[4]*72 Lomitas Road, Danville, CA 94526, USA,*

Abstract

A recently introduced stochastic model for reduced numerical simulation of primary jet breakup is evaluated by comparing model predictions to DNS results for primary jet breakup under diesel conditions. The model uses one-dimensional turbulence (ODT) to simulate liquid and gas time advancement along a lateral line of sight. This one-dimensional domain is interpreted as a Lagrangian object that is advected downstream at the jet bulk velocity, thus producing a flow state expressed as a function of streamwise and lateral location. Multiple realizations are run to gather ensemble statistics that are compared to DNS results. The model incorporates several empirical extensions of the original ODT model that represent the phenomenology governing the Weber number dependence of global jet structure. The model as previously formulated, including the assigned values of tunable parameters, is used here without modification in order to test its capability to predict various statistics of droplets generated by primary breakup. This test is enabled by the availability of DNS results that are suitable for model validation. Properties that are examined are the rate of bulk liquid mass conversion into droplets, the droplet size distribution, and the dependence of droplet velocities on droplet diameter. Quantities of greatest importance for engine modeling are found to be predicted with useful accuracy, thereby demonstrating a more detailed predictive capability by a highly reduced numerical model of primary jet breakup than has previously been achieved.

1. Introduction

Most concepts for current and future high efficiency, low emission internal combustion engines use direct injection of fuel via sprays. Understanding the breakup of the fuel spray is of high interest to further improve engine combustion. When fuel is injected into the engine, the relatively low density ratio between liquid fuel and gas creates strong aerodynamic interactions. The liquid surface becomes unstable and droplets are formed. This process is called primary breakup. Droplets formed from primary breakup break into smaller and smaller droplets in a process called atomization. Fuel droplets evaporate and the fuel vapor mixes with the ambient air to form a fuel-air mixture which ignites either via self-ignition (diesel engine) or spark ignition (gasoline engine). Complete control of fuel-air mixing from primary breakup to turbulent mixing of the fuel vapor with the air in the cylinder is of utmost importance to achieve clean and efficient combustion. As the highly consequential first step in this process, primary breakup plays a special role but is the least well understood.

Due to its technical importance, the breakup of turbulent jets has been investigated experimentally in great detail and many models have been proposed to simulate the breakup process. Eulerian-Lagrangian models are the current workhorses for practical engineering simulations of spray processes including fuel injection in engines. In the majority of these simulations primary breakup is not actually simulated. Instead, simple liquid blobs of the size of the injector diameter are introduced into the simulation. Further breakup of these blobs via secondary breakup is simulated with phenomenological models such as the Taylor analogy breakup (TAB) (O'Rourke and Amsden, 1987; Tanner, 1997) or wave models (Reitz, 1987). Nevertheless, due to the limited understanding of primary breakup, current numerical spray models for Reynolds-averaged Navier-Stokes simulations (RANS) or large-eddy simulations (LES) involve significant

2

simplifications, and tuning is usually necessary every time the flow conditions are changed to achieve satisfactory results.

³⁰ The limited understanding of primary breakup is due to the fact that experimental observation of the high-density region close to jet inlet is extremely difficult. As a result, much of the underlying physics leading to primary breakup is still unclear. Recently, sophisticated imaging techniques such as ballistic imaging and high speed shadow imaging have been able to provide more details of

³⁵ the primary breakup region (Linne, 2013; Rahm et al., 2015). Those new imaging techniques support the development of more predictive primary breakup models.

Direct numerical simulations (DNS) or high resolution large-eddy simulations (LES) offer an alternative way to study liquid-gas interface dynamics dur-

⁴⁰ ing primary breakup. Spatial and temporal resolution is limited only by the available computational resources, which have improved significantly over the past decades. Ménard et al. (2007) and Lebas et al. (2009) performed detailed simulations of jet breakup using a coupled level set/volume-of-fluid method with a ghost fluid approach. However they did not provide quantitative comparisons

⁴⁵ such as droplet size distributions with experimental data. Desjardins et al. (2010) and Desjardins et al. (2013) simulated the primary breakup using a conservative level set/ghost fluid approach. They used realistic turbulent boundary conditions at the injector inflow but no droplet size distributions were reported. Herrmann (2011) studied primary breakup of turbulent liquid jet under diesel

⁵⁰ conditions using the refined level set grid approach. He reported droplet size distributions and results of a grid refinement study providing detailed physical insight into primary breakup for moderate Weber and Reynolds numbers, which is difficult to acquire with experimental studies. However, routine use of DNS for industrial ranges of Weber and Reynolds numbers is still beyond the

⁵⁵ capacity of today's computers (Herrmann, 2010).

For practical simulations of engineering interest as well as to investigate the physics and scalings of primary breakup beyond the parameter range of DNS studies, a predictive and computationally affordable low-order model for

3

simulating primary breakup is highly desirable. For this purpose, the one-dimensional turbulence (ODT) model has been proposed recently by Movaghar et al. (2017) as a primary breakup model. This stochastic modeling approach provides high lateral resolution by affordably resolving all relevant scales in that direction. The low computational cost of ODT compared to fully resolved three-dimensional DNS overcomes the limitation of DNS to moderate Reynolds and Weber numbers. As Movaghar et al. (2017) showed, after parameter tuning ODT has the capability to reproduce the results of experiments by Wu and Faeth (1995) and Sallam et al. (2002) for cases with high liquid/gas density ratio ($\rho_l/\rho_g > 500$). However, under real engine conditions liquid/gas density ratios are relatively low and aerodynamic effects have a significant effect on primary breakup.

In this work we apply the ODT approach presented in Movaghar et al. (2017) to the simulation of primary breakup of a round turbulent liquid jet injected into stagnant high pressure air under diesel-engine-like conditions. The main results, presented in the form of droplet size and velocity distributions as well as an axial profile of the mass rate of conversion from bulk liquid to droplets, are compared to the DNS study of Herrmann (2011).

The flows investigated in this study are governed by the incompressible Navier-Stokes equations for immiscible two-phase flow. The momentum equation is given by

$$\frac{\partial u}{\partial t} + u \cdot \nabla u = \frac{1}{\rho}\nabla p + \frac{1}{\rho}\nabla \cdot [\mu(\nabla u + \nabla^T u)] + \frac{1}{\rho}T_\sigma, \tag{1}$$

where u is the velocity, ρ the density, p the pressure, μ is the dynamic viscosity and T_σ the surface tension force which is nonzero only at the phase interface. All fluid properties are considered to be constant in each phase, allowing the viscous term to be simplified as shown below.

The one-dimensional turbulence model is outlined briefly in section 2. A complete descriptions of the ODT formulation used here is provided in Movaghar et al. (2017). The DNS formulation is discussed in detail in Herrmann (2008).

4

2. One-dimensional turbulence model

ODT is a stochastic model simulating the evolution of turbulent flow along a notional line of sight through a three-dimensional flow. Here it is used to simulated a nominally planar jet. The round-jet interpretation of this planar configuration is explained in Movaghar et al. (2017) and additional details of the execution of the simulations are discussed in Section 3.2. Denoting the jet streamwise direction as x, the ODT line of sight is oriented in the lateral (y) direction. This setup provides high lateral resolution of the relevant physics near the interface.

A Lagrangian picture is adopted, such that time advancement of ODT processes is interpreted as streamwise advancement based on assumed streamwise displacement of the ODT domain at the jet bulk velocity, denoted u_{bulk}. Taking the jet inlet to be the time origin in the ODT simulation, the ODT state at any later time t is interpreted as the state of the jet at streamwise location $x = u_{bulk}t$. Since the ODT state at given t represents the profile in y of all properties that are time advanced during the simulation, a single ODT realization can be interpreted as a representation of the instantaneous state of the jet in the x-y plane. (In Movaghar et al. (2017), an array of y profiles of streamwise velocity, plotted at various x locations, illustrates this interpretation.) Each simulated ODT realization is initialized at the jet inlet with a size-D interval of liquid, where D is the inlet diameter of the round jet represented by the ODT simulation, and gas on both sides of the liquid.

Viscous transport on the ODT line is time advanced by solving

$$\partial u_i(y,t)/\partial t = \nu \partial^2 u_i(y,t)/\partial y^2, \tag{2}$$

where u_i with $i \in 1, 2, 3$ are the three velocity components and ν is the kinematic viscosity. The right-hand side of Eq. (2) is a specialization of the viscous transport in Eq. (1) based on the stated assumption of fixed fluid properties in each phase. A different ν value is needed in each of the phases and the liquid-gas

density ratio is involved in the interfacial momentum-flux matching condition. Consistent with the idealized nature of the flow modeling, the gas-phase flow is parameterized rather than time advancing it using Eq. (2), as explained in Movaghar et al. (2017).

In ODT, turbulent advection is modeled by a stochastic sequence of events. These events represent the impact of turbulent eddies on property fields (velocity and any scalars that might be included) along the one-dimensional domain. During each eddy event, an instantaneous map termed the 'triplet map,' representing the effect of a turbulent eddy on the flow, is applied to all property fields. It occurs within the spatial interval $[y_0, y_0 + l]$, where y_0 represents the eddy location on the ODT line and l is the eddy size. A triplet map shrinks each property profile within $[y_0, y_0 + l]$, to one-third of its original length, pastes three identical compressed copies into the eddy range, and reverses the middle copy to ensure the continuity of each profile. The map mimics the eddy-induced folding effect and increase of property gradients. Formally, the new velocity profiles after a map are given by

$$\hat{u}_i(y, t) = u_i(f(y), t), \tag{3}$$

here conveniently expressed in terms of the inverse map

$$f(y) = y_0 + \begin{cases} 3(y - y_0), & \text{if } y_0 \leq y \leq y_0 + (1/3)l, \\ 2l - 3(y - y_0), & \text{if } y_0 + (1/3)l \leq y \leq y_0 + (2/3)l, \\ 3(y - y_0) - 2l, & \text{if } y_0 + (2/3)l \leq y \leq y_0 + l, \\ y - y_0, & \text{otherwise}, \end{cases} \tag{4}$$

115 which is single-valued. (The forward map is multi-valued.)

The triplet map is measure preserving, which implies that all integral properties of the flow field, such as mass, momentum and kinetic energy, are identical before and after applying the map. Various cases, such as buoyant stratified flow, involve sources and sinks of kinetic energy due to equal-and-opposite changes of

120 one or more other forms of energy. Even in the simplest cases, viscosity converts kinetic energy into thermal energy. The resulting dissipation of kinetic energy

6

is captured by Eq. (2). Energy-conversion mechanisms other than viscous dissipation are incorporated by introducing an additional operation during the eddy event.

In the present formulation, the triplet map can increase the number of phase interfaces within the eddy interval, as illustrated in section 2.3, resulting in an increase ΔE_σ of surface-tension energy that must be balanced by an equal-and-opposite decrease of kinetic energy ΔE_{kin}, such that the total eddy-induced energy change $\Delta E = \Delta E_{kin} + \Delta E_\sigma$ is zero.

Accordingly, the formal statement of the eddy-induced flow change is generalized to

$$\hat{u}_i(y, t) = u_i(f(y), t) + c_i K(y) + b_i J(y) \tag{5}$$

and

$$\hat{\rho}(y, t) = \rho(f(y), t). \tag{6}$$

Here, $K(y) \equiv y - f(y)$ is the map-induced displacement of the fluid parcel that is mapped to location y and $J(y) \equiv |K(y)|$.

Equation (6) indicates that density is triplet mapped but is not subject to addition of the kernels J and K, reflecting the fact that incompressible advection, and therefore its representation by eddy events, does not change the density ρ of fluid elements. (As noted, ρ for given y and t has one of the two values ρ_l and ρ_g.)

The six coefficients b_i and c_i are evaluated by enforcing the prescribed kinetic-energy change based on the surface-tension energy change E_σ, which is zero if the eddy interval contains only one phase. Momentum conservation in each direction i implies three more constraints. The two additional needed constraints are obtained by modeling the eddy-induced redistribution of kinetic energy among the velocity components. In accordance with return-to-isotropy phenomenology, these additional constraints impose a degree of equalization of the component kinetic energies.

7

2.2. Eddy selection

ODT samples eddy events from an eddy event rate distribution that depends on the instantaneous flow state and therefore evolves with the flow. Thus, there is no predetermined frequency of occurrence of eddy events collectively nor of a particular eddy type corresponding to a given location y_0 and size l.

The mean number of events during a time increment dt for eddies located within the interval $[y_0, y_0+dy]$ in the size range $[l, l+dl]$ is denoted $\lambda(y_0, l; t) \, dy_0 \, dl \, dt$. The relation

$$\lambda(y_0, l; t) = C/(l^2 \tau(y_0, l; t)). \tag{7}$$

defines an adjustable parameter C that scales the overall eddy frequency and an eddy time scale τ, where the argument t appearing on both sides of the equation indicates that both λ and τ vary with time for given values of y_0 and l because τ depends on the time-varying instantaneous flow state in the manner described next. (With this understanding, the arguments of τ are henceforth suppressed.) The dimensions of the event rate distribution λ are $(\text{length}^2 \times \text{time})^{-1}$. To find the eddy time scale τ, the square of the implied eddy velocity l/τ is modeled as

$$(l/\tau)^2 \sim E_{final} - Z(\nu^2/l^2), \tag{8}$$

where the first term, which is dependent on the instantaneous flow state, is specified by Eq. (12) in section 2.3 and the second term involving the parameter Z suppresses unphysically small eddies. (The coefficient implied by the proportionality is absorbed into C.) In practice it would be computationally unaffordable to reconstruct the rate distribution every time an eddy event or an advancement of Eq. (2) takes place. Therefore eddy events are sampled using an equivalent Monte-Carlo numerical procedure called thinning (Ross, 1996).

2.3. Multiphase eddy implementation in ODT

As discussed in section 2.1, if the eddy range contains one or both of the liquid-gas interfaces, the eddy is treated as a multiphase eddy. Fig. 1.a shows an eddy that contains a phase interface and hence is a multiphase eddy. Based
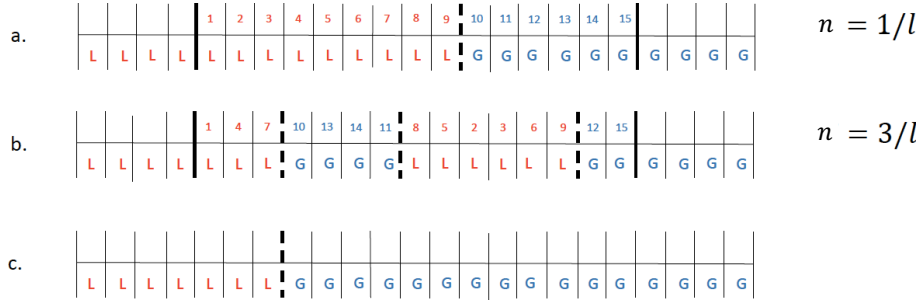
Figure 1: Multiphase eddy treatment in ODT. (a) The size-l spatial region between the thick solid lines is selected for eddy implementation. It is a multiphase eddy containing both liquid (L) and gas (G) separated by one phase interface (thick dashed line), corresponding to $n = 1/l$. (b) A triplet map is implemented here as a permutation of the cells of a uniform spatial discretization of the 1D domain, illustrated by the reordering of cell indices within the eddy. Now there are three phase interfaces, corresponding to $n = 3/l$ and thus $\delta = 2/l$. (c) The newly formed droplet is removed and replaced by gas. Information about removed droplets can be transferred to a secondary-breakup sub-model within a comprehensive spray simulation.

on the main hypothesis of turbulent breakup theory, droplets can be formed by turbulent eddies only when the kinetic energy of the velocity fluctuations is larger than the surface-tension energy required to form a droplet of size corresponding the eddy that produces it. This needs modeling in ODT to account for the eddy-induced change of surface-tension energy.

Incorporation of this into ODT starts from the volumetric density $\sigma\alpha$ of surface-tension energy, where σ is the surface-tension energy per unit area and α is the surface area per unit volume. This gives an energy density

$$E_\sigma = \sigma\alpha/\bar{\rho} \tag{9}$$

per unit mass, where $\bar{\rho}$ is the mean density. The meaning and evaluation of α and $\bar{\rho}$ in ODT are considered.

Since an interface in ODT is represented by an isolated point on a line, geometric interpretation is required in order to obtain the area increase in the case of breakup. A plausible assumption for highly turbulent cases involving wrinkled interfaces is that the interface is a statistically homogeneous isotropic

9

random surface. For such a surface, a number density n of interface intersections along a line of sight corresponds to an interface area per unit volume $\alpha = 2n$ (Chiu et al., 2013). On this basis,

$$E_\sigma = 2n\sigma/\bar{\rho}. \tag{10}$$

This assumption might not be precisely accurate for the jet breakup problems considered here, but it is convenient to adopt it as a universal assumption rather than to attempt a case-by-case treatment. The assumption is used only to evaluate E_σ for jet-breaking eddies, which are typically small relative to the jet diameter in the axial range considered here. The tendency for the turbulent cascade to induce small-scale homogeneity and isotropy is well established (Goto and Kida, 2003, 2007).

Because there are always exactly two phase interfaces on the ODT domain at the inception of an eddy event, the number of interfaces within any eddy is 0, 1, or 2, corresponding to number densities $n = 0$, $1/l$ or $2/l$, respectively, within the eddy. Triplet mapping of a phase interface within an eddy produces three such interfaces. This is shown in Fig. 1.b and is interpreted as a tripling of interfacial area. The eddy-induced increase δ of the number density of interfaces due to triplet mapping which will be 0, $2/l$ or $4/l$ for the mentioned cases. Based on the relation $\alpha = 2n$, the interfacial area increase per unit volume is 2δ. Multiplication by the surface tension σ gives the surface tension potential energy per unit volume that is stored in the newly created interfaces. This implies the surface tension energy change per unit mass

$$\Delta E_\sigma = 2\sigma\delta/\bar{\rho}, \tag{11}$$

where $\bar{\rho}$ is now identified as the mean density with the eddy range. This explanation corrects an erroneous discussion of these points in Movaghar et al. (2017), but the final result, Eq. (11), is unchanged.

Conservation of total energy requires an equal and opposite change of the final kinetic energy. Here this implies

$$E_{final} = E_{kin} - \Delta E_\sigma, \tag{12}$$

10

where E_{kin} and E_{final} are the available kinetic energy per unit mass before and after the change, respectively. Here, available means the maximum amount extractable by adding weighted J and K kernels to the instantaneous velocity profiles as shown in Eq. (5). The change is implemented by similarly modifying the velocity profiles using weighted J and K kernels, but in this instance extracting the energy ΔE_σ from the flow field within the eddy interval, as described in section 2.1.

As we focus on modeling primary breakup, droplets are removed from the computational domain as triplet maps create them by separating liquid from the jet, see Fig. 1.b. Fig. 1.c shows that the resulting gaps are set to gas-phase conditions. Except for breakup events that contain the entire liquid region (the model analog of liquid-column disintegration), a triplet map can create only one droplet.

Droplets are removed because there is no suitable way to time advance their motion and interactions on the 1D Lagrangian domain. In any case, their subsequent fate is a question beyond the scope of the primary-breakup phenomenon addressed here. The ultimate purpose of the ODT primary-breakup model is to use the statistics of the released droplets as inputs to a spray model of conventional form that then time advances droplet populations using probability distribution functions or other standard tools. With such coupling, the spray model could be used to characterize the droplet-laden gaseous medium in the ODT primary-breakup model, resulting in two-way coupling of the primary-breakup model and the spray model.

The above description covers the essentials of the ODT primary-breakup formulation. In order to capture global features of breaking liquid jets such as the Weber-number dependence of the liquid column length, Eq. (8) was supplemented with additional terms idealizing the Rayleigh and aerodynamic-shear mechanisms of liquid-column disintegration. The present study retains all these details, including the assigned values of adjustable parameters, as described in Movaghar et al. (2017), so the reader is referred to that publication for a complete discussion. The intent here is to determine the extent to which this

11

formulation, designed and validated with reference to global jet structure, is able to capture local features such as the size distribution of droplets produced by primary breakup.

3. Operating conditions and computational setups

3.1. Operating conditions and DNS computational setup

Simulations have been performed of the primary breakup of a turbulent liquid jet injected into stagnant dense air under diesel engine conditions. Figure 2 shows the cylindrical DNS computational domain. It extends 20 inlet diameters D downstream of the jet inlet and 4 diameters in the radial direction.
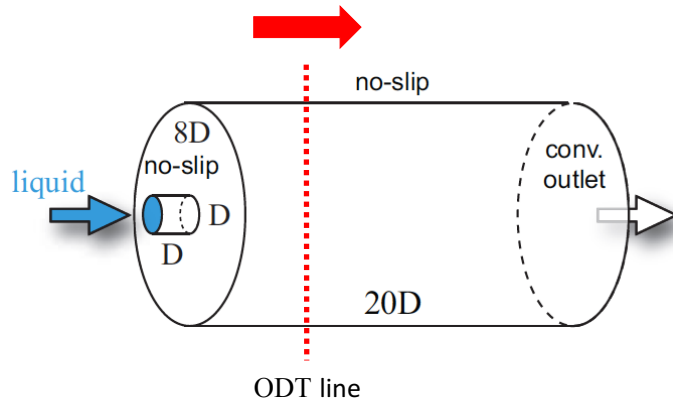

Figure 2: DNS and ODT computational setups.

In the DNS, which is described in detail in Herrmann (2011), no-slip boundary conditions are used on all boundary faces, except for a convective outflow at the right boundary and an inflow boundary condition at the injector pipe inlet. To accurately represent the turbulence of the liquid at the inlet, DNS of single-phase periodic pipe flow was performed using the injector-flow Reynolds number $Re_{bulk} = 5000$. The DNS results were stored in a database and then used as inflow boundary conditions for the atomization simulation.

Table 1 summarizes the operating conditions used in the simulations. The gas phase is initialized to be motionless.

Parameter	Value
μ_l (Liquid absolute viscosity)	1.7×10^{-3} kg/ms
μ_g (Gas absolute viscosity)	1.78×10^{-5} kg/ms
D (Initial jet diameter)	100 μm
u_{bulk} (Jet inlet mean velocity)	100 m/s
ρ_l/ρ_g (Liquid/gas density ratio)	34
$Re_{bulk} = \rho_l u_{bulk} D / \mu_l$ (Reynolds)	5000
$We = \rho_l u_{bulk}^2 D / \sigma$ (Weber)	17000
$Oh = \mu_l / (\rho_l D \sigma)^{0.5}$ (Ohnesorge)	0.026

Table 1: Simulation conditions for the liquid jet.

3.2. ODT computational setup

As explained in section 2.1 and illustrated in Fig. 2, the ODT line is interpreted as a Lagrangian object advected downstream at velocity u_{bulk} during a
230 simulated realization. The ODT simulation setup in this study involves first, the generation of initial property profiles at the jet inlet plane, and second, the time advancement of the jet breakup simulation.

The initial velocity profiles u_i for the jet breakup simulation are obtained by performing a channel-flow simulation representing the turbulent flow in the
235 injector pipe. During the channel-flow simulation, Dirichlet boundary conditions are applied at both endpoints of the ODT line (representing no-slip wall boundary conditions) and the ODT parameters are chosen to be C = 5.2 and Z = 10 as in Movaghar et al. (2017). The ODT flow state at the end of the channel simulation is saved for initialization of the next simulated channel-flow
240 realization that generates a new initial condition for the next jet simulation.

With this procedure, each profile at the jet inlet plane represents an instantaneous flow state along a wall-normal line of sight within a fully developed channel flow. (See the cited reference for additional details concerning the model formulation and parameter settings in the jet portion of the simulation.) Each
245 simulated ODT realization of the jet is performed for a computational time

13

corresponding to a streamwise distance $x/D = 20$, which is the axial extent of the DNS domain. Statistics are presented either as a function of x/D or on the basis of all droplets generated by the ensemble of simulations.

The ODT results presented here are based on an ensemble of 10000 simulated realizations, corresponding to a total CPU time of 24 hours, which is lower by a factor of 10000 than the CPU time for the DNS comparison case. This doesn't fully indicate the cost advantage of ODT because adequate statistics could have been obtained with significantly fewer simulated realizations, but 10000 realizations were nevertheless run because it was convenient to do so. (For visual clarity, scatter plots shown here are based on data from 500 realizations. Those plots demonstrate that fewer realizations are sufficient for ample output statistics.) However, the DNS run time cannot be substantially reduced without reducing numerical accuracy and thereby degrading the fidelity of the results.

As discussed by Herrmann (2011), in the DNS it takes approximately 4 μs for the turbulent pipe flow to reach the jet inlet plane and thereafter influence the liquid/gas interface. Before this stage, breakup occurs in a fully laminar environment and by mechanisms that are beyond the scope of this paper. For the comparison we limit ourselves to conditions of statistically stationary turbulent breakup. The ODT formulation is inherently limited to representation of statistically stationary conditions because ODT time advancement is a surrogate for streamwise advancement according to the Lagrangian interpretation adopted here, so there is no representation of transient jet development at a given streamwise location.

4. Results

4.1. Droplet mass generation rate

The most basic quantitative signature of primary breakup is the rate of liquid jet mass loss due to droplet generation by primary breakup. Figure 3 shows the cumulative jet-to-droplet mass conversion rate $\dot{m}_d$ as a function of x/D, meaning that $\dot{m}_d$ for given x/D is the axial mass flux of all droplets

generated between the jet inlet and x/D. In the plot, $\dot{m}_d$ is normalized by the liquid jet mass flux $\dot{m}_0$ at the jet inlet plane.
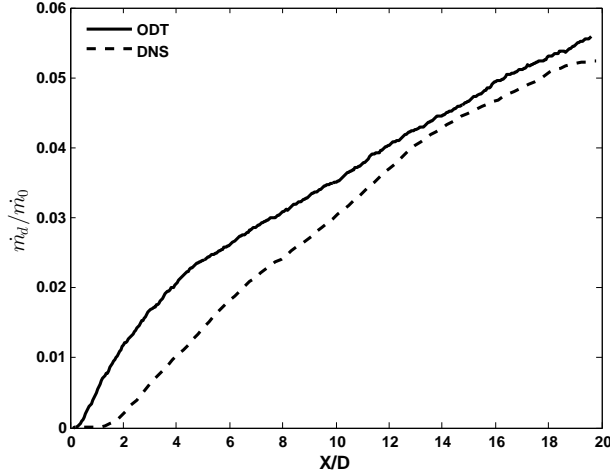

Figure 3: Cumulative jet-to-droplet mass conversion rate due to primary breakup normalized by the liquid jet mass flux at the jet inlet plane.

In the far field, the ODT results agree quite well with the DNS. The main difference between the two curves is that the near-field jet-to-droplet mass conversion rate is larger for ODT than for DNS, followed by bending of the ODT curve to a shallower slope near $x/D = 4$, while for DNS this bending does not occur until $x/D = 13$. The ODT near-field conversion rate is thus higher than for DNS, but does not extend as far as the DNS near-field transient before bending to a lower rate. These two effects nearly cancel, such that the ODT droplet mass flux at $x/D = 13$ nearly matches the DNS value, after which the nearly equal (and roughly constant) slopes of the two curves indicate that the ODT far-field conversion rate is equal to the DNS rate within the statistical precision of the curves.

There are at least two possible causes of the near-field discrepancies. One is that the transition at the jet inlet plane from confined flow with no-slip walls to a free liquid interface coupled to the gas flow is likely to induce local three-dimensional pressure fluctuations beyond the scope of phenomenology captured

15

by ODT. Another is that primary breakup is deemed to occur in ODT at the instant of separation of a liquid parcel from the jet, but in the DNS, such separation is primarily by ligament formation, and droplet formation is deemed to occur only when droplets separate from the ligaments. This delays the attribution of liquid mass loss until larger x/D, which might partially explain the shallower but more extended near-field transient indicated by the DNS. In principle it is possible to introduce an analogous delay of mass-loss attribution in ODT that might bring the near-field results into better agreement. However, this would be only a bookkeeping adjustment that does not introduce any physically based representation of droplet generation mediated by ligament formation into ODT. Moreover, it would involve model and parameter adjustments that would deviate from the present focus on strictly predictive application of the previously reported model formulation. For these reasons, it is not attempted here.

With regard to prediction, two points are noteworthy. First, the model was designed and validated with emphasis on the global jet structure, as explained in section 2.3, but the comparisons in Fig. 3 and results that follow focus on local details of breakup that test the broader applicability of the model. Second, the lower ρ_l/ρ_g value for the present case than for the ambient-pressure cases previously used to calibrate the model tests the robustness of its parameter-space extrapolation.

4.2. Droplet size distribution

One of the main outputs of the primary-breakup simulations is droplet-size information. Due to its computational affordability, ODT can be used in the future to generate droplet-size distributions as inputs for a standard Lagrangian spray model.

ODT is numerically implemented using a specially designed adaptive mesh that does not limit the droplet size resolution, so arbitrarily small droplets can be released, as prescribed by the physics. Neither the numerics nor the physical modeling inherently constrain the range of droplet sizes whose primary

16

breakup can be predicted using ODT, but model simplifications and omissions of physical mechanisms that influence the process imply that the predictions cannot be deemed reliable without adequate validation. The present study compares ODT predictions to DNS results as a contribution to this objective.

In DNS (or any grid based method) simulations generally, the minimum size of droplets depends on the grid size - droplets smaller than the grid size cannot be represented by interface tracking methods such as volume of fluids (VOF) or level-set methods unless using inherent subgrid resolution as described by Herrmann (2008). In Herrmann (2011) the resolution of the level set is finer than the flow solver to minimize the impact of the grid size on the breakup process. A grid resolution of $0.0039D$ is used for resolving the interface and $0.01D$ for the flow. For comparison, a similar resolution should be used for the ODT simulations. We have chosen the smallest eddy size allowed in the ODT simulation to be $0.002D$ and suppress all eddies of smaller size (though the generation of smaller droplets is still not completely ruled out because an eddy can overlap an arbitrarily small liquid interval and form a droplet from a portion of that interval).

As discussed in section 2.3, a multiphase eddy detaches a liquid interval of some length l_d from the bulk liquid. For breakup of a round jet, the ODT droplet size is not the same as the length of the liquid interval l_d. Instead we define $S = Bl_d$ as the size of the droplet, where B is a tunable coefficient. In Movaghar et al. (2017), tuning of B to match measurements of high-density-ratio (ambient-pressure) jet breakup gave the optimum value $B = 0.2$. The same value is used here in order to test the robustness of that parameter fit (and of the other features of the ODT formulation).

On this basis, Fig. 4 shows the droplet-size probability density function $f(D)$ resulting from primary breakup in DNS and ODT simulations. The distributions are histograms that partition the diameter range into 20 bins. The results show good agreement of the ODT and DNS results, notably including the relatively rare production of large droplets.

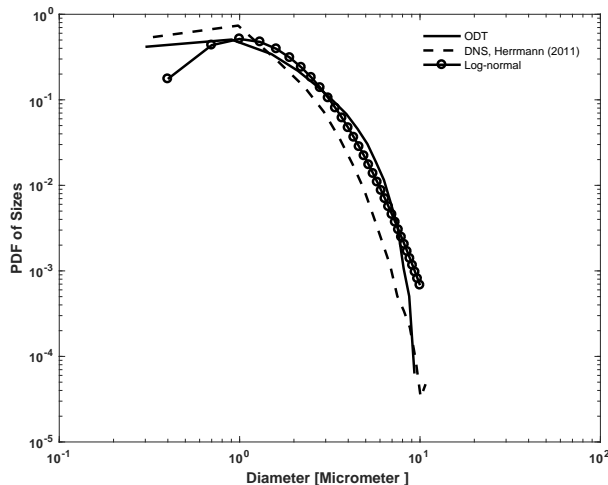Fig. 4 shows also a log-normal distribution fitted to the ODT results. It

17

Figure 4: Droplet size distribution.

provides a rough but reasonable representation of the ODT distribution. Thus, if ODT is used to develop a parameterized tabulation of droplet size distributions, log-normal fits might be suitable for condensing the information, e.g. for use in subgrid closures of coarse-grained simulations of primary atomization.

Since Fig. 4 is based on the aggregate of droplets throughout the x/D range $[0, 20]$, it doesn't reflect variation of the size distribution as the jet develops spatially. To capture this, several representations of the streamwise variation of droplet statistics are presented.

First, in Fig. 5, DNS and ODT results for $f(D)$ are shown for two subranges of the streamwise range of the simulations. It is seen that there is little difference between the distributions in the two subranges. Further subdivision of the near-field data into x/D subranges $[0, 5]$ and $[5, 10]$ (not shown) indicates some greater degree of x/D dependence of the ODT results but hardly any such dependence of the DNS results. However, the results shown next indicate transient behaviors not captured by this comparison.

Droplet Sauter Mean Diameter (SMD) is shown as a function of x/D in Fig. 6. There is rough (30% maximum deviation) quantitative agreement of ODT with the DNS results at all x/D, but reflecting the observation in the
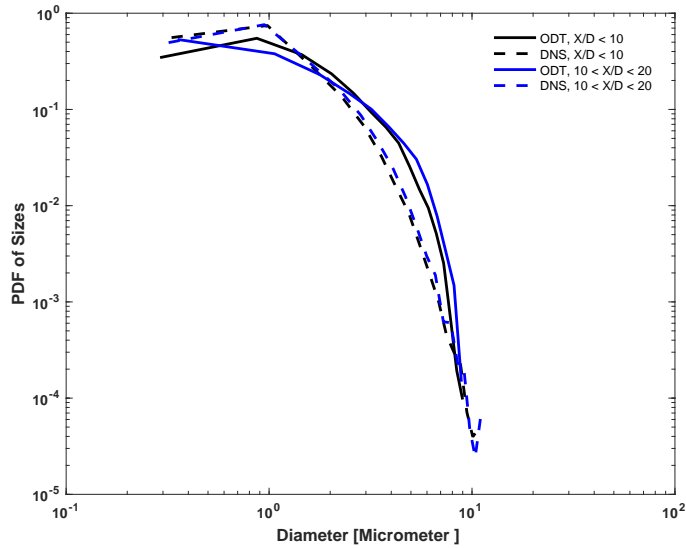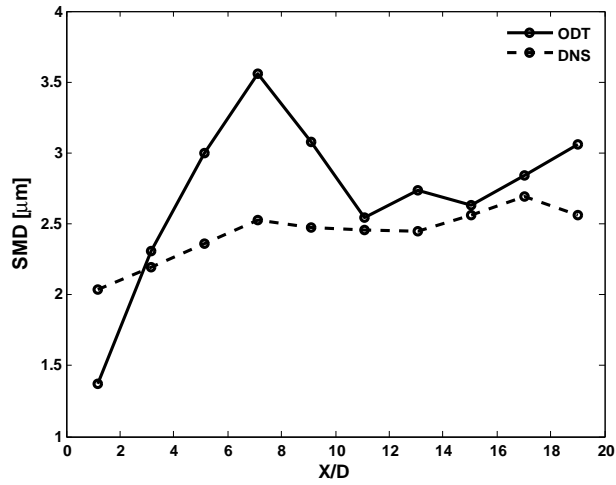
18

Figure 5: Droplet size distribution

Figure 6: Droplet Sauter Mean Diameter (SMD) versus distance from the jet inlet.

previous paragraph, ODT shows markedly greater near-field x/D dependence than the DNS.

To examine these tendencies in greater detail, scatter plots of droplet diameter versus x/D are shown in Fig. 7. The main difference between the ODT and DNS results is the absence of significant droplet generation for $x/D < 1$
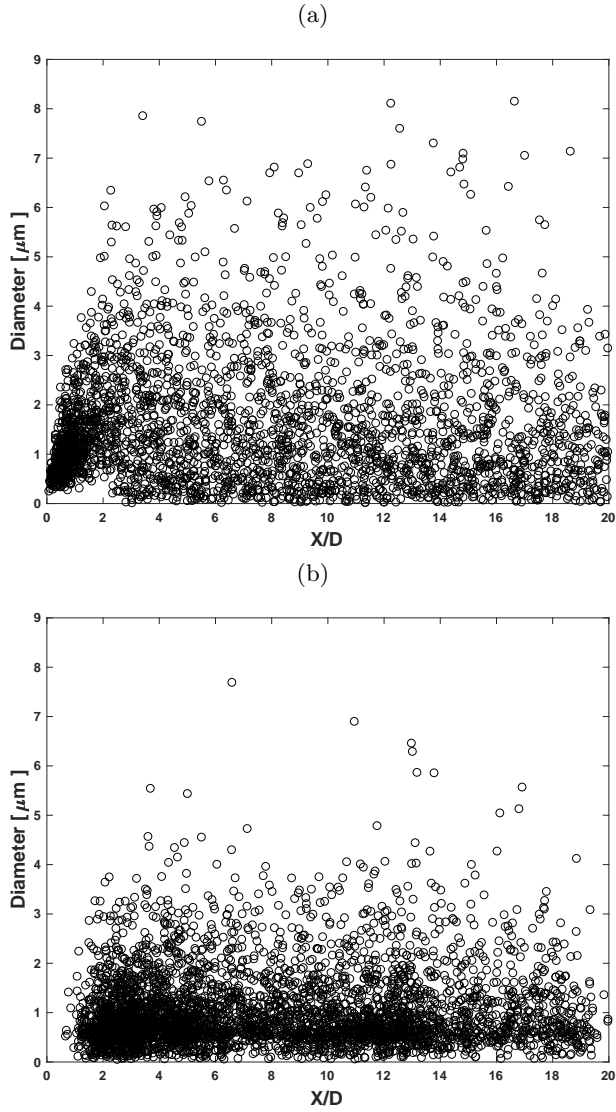
19

(a)

(b)

Figure 7: Scatter plots of droplet diameter versus distance from the jet inlet. (a) ODT, (b) DNS.

in the DNS, while the ODT results indicate no discernible delay of the onset of droplet generation.

Parameter dependences of the x/D value for onset of droplet generation were examined in Movaghar et al. (2017) for ambient pressure conditions cor-

20

responding to a liquid/gas density ratio of order 1000. In that case, ODT was found to underestimate the onset distance by roughly a factor of two relative to experimental results for values of Reynolds number and Weber number close to those for the present case. (Onset distance was defined as the most probable onset location based on the distribution of onset locations generated by an ensemble of ODT realizations. The median of this distribution likewise gave an underestimate, but was not as far below the measurements.)

For the present case, the liquid/gas density ratio is lower and both DNS and ODT indicate onset closer to the inlet than for ambient conditions, with ODT again underestimating the onset distance. The implication is that aerodynamic coupling, which is enhanced by an increase of the gas density, promotes early onset of droplet generation. ODT appears to exaggerate this tendency.
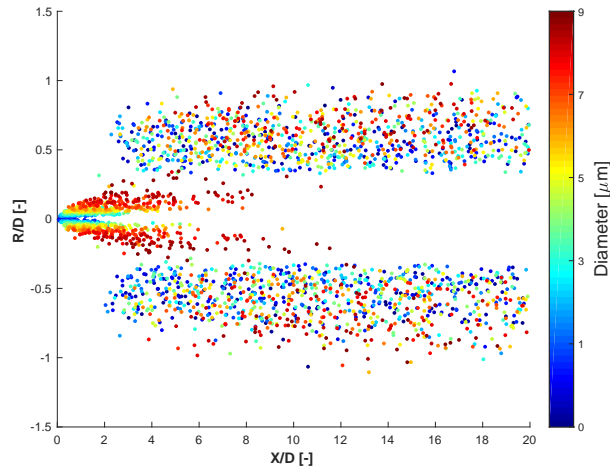

Figure 8: ODT droplet spatial distribution, where the ordinate is the distance R of a droplet from the jet perimeter immediately after droplet formation, scaled by D, and the color bar indicates the droplet diameter in μm.

The ODT behavior is further elucidated by Fig. 8, which is a scatter plot of axial and lateral droplet location, with lateral location expressed as droplet distance R from the jet perimeter immediately after droplet formation. Droplet sizes are color-coded.

This plot captures all the information shown in Fig. 7.a as well as the lateral

21

droplet locations relative to the jet perimeter upon droplet formation. However, the available DNS output does not allow a comparable rendering of DNS results, which is why Fig. 7 is also shown.

R/D values provide an indication of the sizes of the droplet-forming ODT eddy events. The small R/D values in the near field reflect the persistence of the channel-flow inlet condition over some x/D range. The thin boundary layers at the edges of the channel flow evolve into regions of high liquid shear in the vicinity of the jet perimeter, albeit decaying due to turbulent transport that spreads velocity fluctuations laterally and droplet generation that removes strongly sheared liquid from the jet, in effect peeling away the boundary layer. This flow structure generates eddies comparable in scale to the thin high-shear regions. Some of these eddies generate droplets at locations that are relatively close to the jet perimeter as seen in Fig. 8, which also shows the gradual reduction of this tendency with increasing x/D.

Farther downstream, a transition to droplet formation by larger eddies is apparent, consistent with decay of the initial shear layers and increasing droplet formation by larger eddies, whose contribution is delayed due to the relatively long turnover times of these eddies. Both liquid bulk turbulence and aerodynamic shear can contribute to the occurrence of such eddies. It is seen that many of the droplets that are generated in the far field are small relative to the size of the eddies that produce them. (Note in Table 1 that $D = 100$ μm.) These eddies are thus located primarily in the gas phase, and hence driven largely by aerodynamic shear, which is thus an important if not dominant cause of far-field droplet generation. Indeed, the aerodynamic shear treatment introduced in Movaghar et al. (2017) is formulated to increase the strength of this droplet-generation mechanism with increasing x/D.

This strengthening droplet-generation mechanism is supplemented by the contribution of liquid bulk turbulence, which decays with increasing x/D. Figures 7.a and 8 indicate that the net effect is gradually decreasing but generally stable droplet generation, as seen also in the DNS results in Fig. 7.b. The slight decreasing tendency is quantified on a mass basis in Fig. 3.

22

The overall impression is that droplet generation by relatively large eddies is reasonably well represented by the model, but there is excessive near-field droplet formation by small eddies induced by locally strong shear originating in the inlet flow. This discrepancy was evident to some extent in previous work focusing on very high liquid/gas density ratios, but is more pronounced in the present model application to a case with a lower, though still high, density ratio. In the model, the gas streamwise velocity is spatially uniform with a value that matches the liquid streamwise velocity at the phase interface. On this basis, higher gas density more effectively counteracts the increase of the liquid velocity at the phase interface caused by lateral homogenization of the liquid jet by bulk turbulence. Therefore inaccurate modeling of the aerodynamic coupling has more severe consequences as the liquid/gas density ratio is reduced. The aerodynamic coupling was formulated in Movaghar et al. (2017) to match far-field rather than near-field behavior, so present results might motivate future modification of the near-field aerodynamic coupling in the model.

Notwithstanding the nuances of aerodynamic coupling, the notion that the liquid-phase contribution to breakup is initially boundary-layer controlled and subsequently controlled by homogeneous turbulence is intrinsically plausible. A recent study that re-examined experimental results on the parameter dependences of liquid-jet breakup onset found evidence supporting the relevance of both of these mechanisms (Kerstein et al., 2017). Though the initial flow state of the liquid is an input to the ODT jet simulation, its subsequent development is governed by the ODT representation of turbulence dynamics, which broadly captures the main features in this as in other model applications.

4.3. Droplet velocity distribution

Figure 9 shows the droplet mean axial velocity conditioned on droplet diameter for ODT and DNS. The distributions are discretized using 10 bins over the range of droplet diameters. The profiles are normalized by the liquid bulk velocity at the jet inlet plane. ODT captures the overall magnitude and trend of the DNS results (note that the vertical origin is a positive value and the
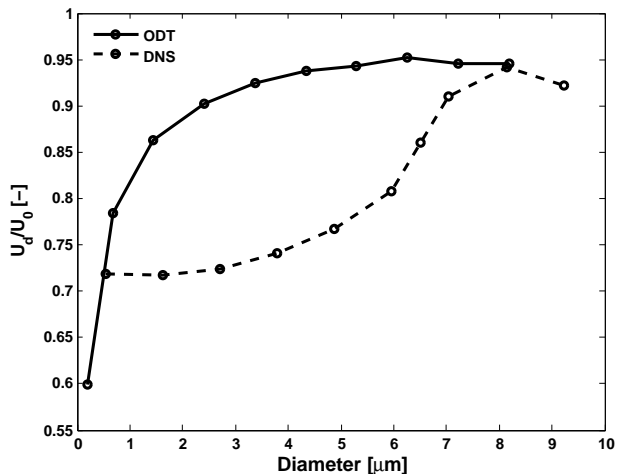
23

Figure 9: Normalized droplet mean axial velocity conditioned on droplet diameter. U_0 is the liquid bulk velocity at the jet inlet.

maximum ODT error is under 30%), but the curves have different shapes.

This may have several reasons but we believe that ligament formation prior to droplet generation, which ODT cannot emulate (as discussed in section 4.1) is the leading effect. Another consideration is that droplet velocities are influenced by the return-to-isotropy representation in ODT that is described in section 2.1. This idealization of an effect stemming from complicated pressure-fluctuation effects is rough at best, so ODT predictions of droplet velocities might be less reliable than droplet-size predictions.

ODT results for a normalized measure of droplet kinetic energy in the plane normal to the axial direction, shown in Fig. 10, grossly underpredict the DNS results. In addition to the possible causes described above, another possible cause of this underprediction is the inability of ODT to capture radial undulations of the liquid-gas interface, which might contribute to the DNS radial velocity.

To further elucidate the parameter dependences of droplet velocity, scatter plots of normalized droplet axial velocity against diameter from ODT and DNS computations are shown in Fig. 11. Color is used to indicate the axial location
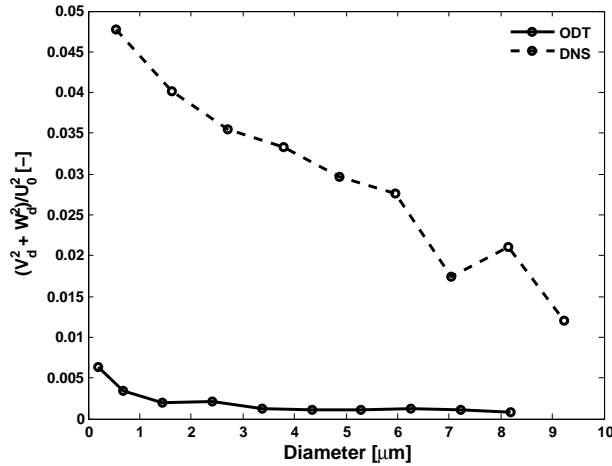
24

Figure 10: Droplet kinetic energy in the lateral plane, conditioned on droplet diameter. The normalizing velocity is defined as in Fig. 9.

475 at the instant of droplet formation, as defined for ODT and DNS in section 4.1.

The ODT scatter plot shows that droplets close to jet inlet have lower axial velocities than droplets farther downstream. This can be explained by the influence of the flow profile of the jet at the jet inlet plane: in the near field the velocities inside the liquid jet near the liquid-gas interface are still dominated 480 by the boundary layer profile leading to low velocities in the droplet-generating region near the interface. Farther downstream, radial turbulent transport within the jet tends to homogenize the lateral profile of axial velocity, thereby increasing it near the liquid-gas interface.

Though this is a physically reasonable trend, the DNS scatter plot indicates 485 that any such trend is dominated by a much larger scatter of velocity values than is produced in ODT. The likely cause is the greater complexity of the three-dimensional breakup process than its one-dimensional ODT analog, as discussed in section 4.1. Notable in this regard is the occurrence of negative axial velocities in Fig. 11.b, which might be due to a viscoelastic action-reaction 490 mechanism when axially oriented ligaments decompose into droplets, propelling some droplets forward (note the large positive axial velocity values) and others backward.
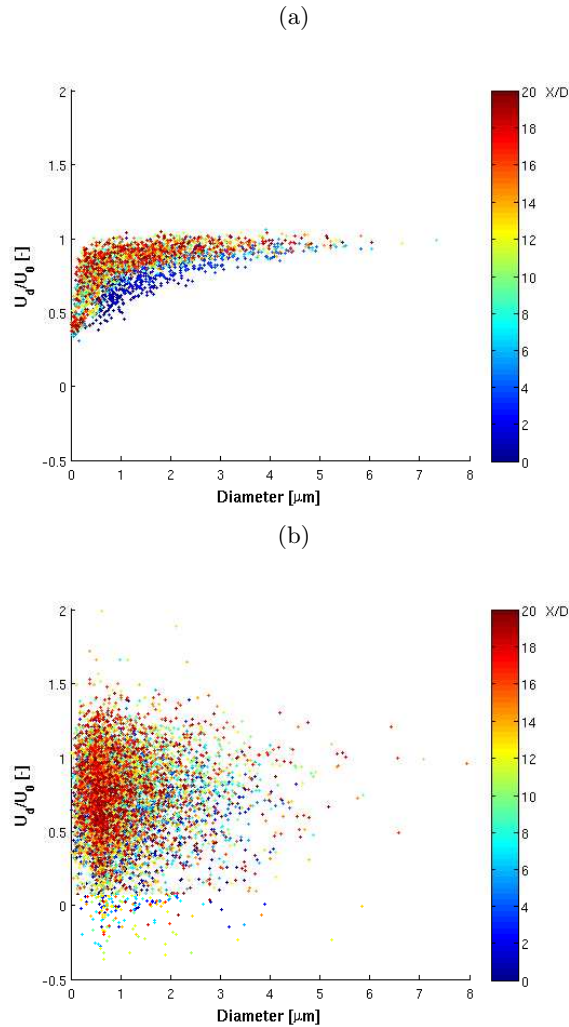
25

(a)

(b)

Figure 11: Scatter plots of droplet axial velocity, normalized by the injection velocity, versus diameter. The color indicates the distance from the jet inlet. (a) ODT, (b) DNS.

5. Conclusion

The recently introduced primary-breakup model of Movaghar et al. (2017)

495 based on the one-dimensional turbulence (ODT) model was used here to simulate the primary breakup of a turbulent jet under diesel-like conditions. The results have been compared to droplet statistics from a direct numerical simu-

lation (DNS).

The results show that ODT reproduces the rate of bulk liquid mass conversion into droplets and the droplet-size distribution produced by the DNS to a useful degree of accuracy. Some quantitative and qualitative discrepancies of the dependence of droplet velocities on droplet diameter were observed.

The significance of the present results stems from the fact that the model formulation of Movaghar et al. (2017) was used here without any modification or parameter resetting. The model involves numerous parameters that were tuned to match global properties, such as the Weber number dependence of the liquid jet length, that were determined experimentally for ambient-pressure conditions. As noted in section 4, an additional parameter was tuned in that study to match measured values of the droplet Sauter mean diameter (SMD) at the onset of breakup over a range of Weber numbers and other SMD measurements as a function of axial location. Though the ability to capture these SMD parameter dependences based on a single parameter adjustment indicates some degree of model fidelity with regard to droplet statistics, this does not constitute a definitive demonstration of quantitative predictive capability.

Having fully specified the model in this manner in previous work, the present evaluation of more detailed droplet statistics produced by ODT by comparing them to DNS results provides a clear assessment of predictive capability. In some important respects, predictive accuracy is confirmed. The lower accuracy of droplet-velocity predictions is understandable in view of the simplified ODT treatment of turbulent energy redistribution among velocity components and the inability of ODT to represent explicitly the effects of ligament formation and destabilization processes that mediate droplet formation.

Indeed, it is perhaps surprising that overall bulk liquid conversion and the droplet-size distribution are so well predicted in view of the latter caveat. To rule out the possibility of agreement due to, e.g., fortuitous cancellation of errors, it will be important to compare ODT predictions to other DNS cases as they become available. Based on the results presented here and in Movaghar et al. (2017), it can nevertheless be concluded that the evidence in hand con-

27

stitutes a more convincing demonstration of detailed predictive capability by

a highly reduced numerical model of primary jet breakup than has previously

been achieved.

Acknowledgments

References

Chiu SN, Stoyan D, Kendall WS, Mecke J. Stochastic geometry and its applications. John Wiley & Sons, 2013.

Desjardins O, McCaslin J, Owkes M, Brady P. Direct numerical and large-eddy simulation of primary atomization in complex geometries. Atomization and Sprays 2013;23:1001–48.

Desjardins O, Pitsch H, et al. Detailed numerical investigation of turbulent atomization of liquid jets. Atomization and Sprays 2010;20:311–36.

Goto S, Kida S. Enhanced stretching of material lines by antiparallel vortex pairs in turbulence. Fluid Dynamics Research 2003;33:403–31.

Goto S, Kida S. Reynolds-number dependence of line and surface stretching in turbulence: folding effects. Journal of Fluid Mechanics 2007;586:59–81.

Herrmann M. A balanced force refined level set grid method for two-phase flows on unstructured flow solver grids. Journal of Computational Physics 2008;227:2674–706.

Herrmann M. Detailed numerical simulations of the primary atomization of a turbulent liquid jet in crossflow. Journal of Engineering for Gas Turbines and Power 2010;132:061506.

Herrmann M. On simulating primary atomization using the refined level set grid method. Atomization and Sprays 2011;21:283–301.

Kerstein AR, Movaghar A, Oevermann M. Parameter dependences of the onset of turbulent liquid-jet breakup. Journal of Fluid Mechanics 2017;811:R5.

Lebas Romain andf Menard T, Beau P, Berlemont A, Demoulin FX. Numerical simulation of primary break-up and atomization: DNS and modelling study. International Journal of Multiphase Flow 2009;35:247–260.

Linne M. Imaging in the optically dense regions of a spray: A review of developing techniques. Progress in Energy and Combustion Science 2013;39:403–440.

Ménard T, Tanguy S, Berlemont A. Coupling level set/vof/ghost fluid methods: Validation and application to 3D simulation of the primary break-up of a liquid jet. International Journal of Multiphase Flow 2007;33:510–24.

Movaghar A, Linne M, Oevermann M, Meiselbach F, Schmidt H, Kerstein AR. Numerical investigation of turbulent-jet primary breakup using one-dimensional turbulence. International Journal of Multiphase Flow 2017;89:241–54.

O'Rourke PJ, Amsden AA. The TAB method for numerical calculation of spray droplet breakup. SAE Technical Paper 1987;872089.

Rahm M, Paciaroni M, Wang Z, Sedarsky D, Linne M. Evaluation of optical arrangements for ballistic imaging in sprays. Optics express 2015;23:22444–62.

Reitz RD. Modeling atomization processes in high-pressure vaporizing sprays. Atomisation and Spray Technology 1987;3:309–37.

Ross SM. Stochastic Processes. 2nd ed. John Wiley & Sons New York, 1996.

Sallam K, Dai Z, Faeth G. Liquid breakup at the surface of turbulent round liquid jets in still gases. International Journal of Multiphase Flow 2002;28:427–49.

Tanner F. Liquid jet atomization and droplet breakup modeling of non-evaporating diesel fuel sprays. SAE Technical Paper 1997;970050.

Wu PK, Faeth G. Onset and end of drop formation along the surface of turbulent liquid jets in still gases. Physics of Fluids 1995;7:2915–7.